Nuclear Engineering and Technology 55 (2023) 222–228

Contents lists available at ScienceDirect

Nuclear Engineering and Technology

journal homepage: www.elsevier.com/locate/net

Original Article

Feasibility study of improved median filtering in PET/MR fusion images with parallel imaging using generalized autocalibrating partially parallel acquisition

Chanrok Park [a], Jae-Young Kim [b], Chang-Hyeon An [c], Youngjin Lee [d,*]

[a] Department of Radiological Science, Eulji University, Gyeonggi-do, Republic of Korea
[b] Department of Biochemistry, School of Dentistry, IHBR, Kyungpook National University, Daegu, Republic of Korea
[c] Department of Oral and Maxillofacial Radiology, School of Dentistry, IHBR, Kyungpook National University, Daegu, Republic of Korea
[d] Department of Radiological Science, Gachon University, Incheon, Republic of Korea

ARTICLE INFO

Article history:
Received 8 August 2022
Received in revised form
4 September 2022
Accepted 15 September 2022
Available online 22 September 2022

Keywords:
Positron emission tomography (PET)
Magnetic resonance (MR)
fusion imaging system
Fast magnetic resonance imaging (MRI)
Generalized autocalibrating partially parallel acquisition (GRAPPA)
Improved median filter
Image quality improvement

ABSTRACT

This study aimed to analyze the applicability of the improved median filter in positron emission tomography (PET)/magnetic resonance (MR) fusion images based on parallel imaging using generalized autocalibrating partially parallel acquisition (GRAPPA). In this study, a PET/MR fusion imaging system based on a 3.0T magnetic field and ^{18}F radioisotope were used. An improved median filter that can set a mask of the median value more efficiently than before was modeled and applied to the acquired image. As quantitative evaluation parameters of the noise level, the contrast to noise ratio (CNR) and coefficient of variation (COV) were calculated. Additionally, no-reference-based evaluation parameters were used to analyze the overall image quality. We confirmed that the CNR and COV values of the PET/MR fusion images to which the improved median filter was applied improved by approximately 3.32 and 2.19 times on average, respectively, compared to the noisy image. In addition, the no-reference-based evaluation results showed a similar trend for the noise-level results. In conclusion, we demonstrated that it can be supplemented by using an improved median filter, which suggests the problem of image quality degradation of PET/MR fusion images that shortens scan time using GRAPPA.

1. Introduction

Anatomical and functional imaging devices are widely used in diagnostic medical imaging [1,2]. Recently, a fusion imaging system that can simultaneously acquire anatomical and functional images was developed. Representative types of fusion imaging systems include positron emission tomography (PET)/magnetic resonance imaging (MRI), PET/computed tomography (CT), and single-photon emission computed tomography (SPECT)/CT [3–6]. Among these imaging devices, PET/MRI uses a positron-emitting nuclide, such as ^{18}F, and has the advantage of acquiring images with a very high resolution compared with those acquired using PET/CT [6]. In addition, compared with CT, MRI has a great advantage in that radiation exposure need not be considered when acquiring anatomical images.

Compared with CT-based fusion imaging systems, MRI-based modalities require a longer scan time [7]. In particular, because it takes as much time as the sum of each scan time of PET and MRI to acquire a PET/MR fusion image, reducing this is a significant challenge for many researchers. Although it is possible to reduce the MRI scan time by reducing the number of samplings in k-space, aliasing inevitably occurs, thereby reducing the diagnostic accuracy [8]. Parallel imaging using a multichannel coil is widely used to overcome these shortcomings [8–10]. Generalized autocalibrating partially parallel acquisition (GRAPPA), one of the most representative methods of parallel imaging, is based on the principle of estimating coil-sensitivity profiles by fully sampling the center of the k-space and sparsely obtaining the edge [10,11]. Fig. 1 shows a schematic diagram of a simple GRAPPA approach in a brain MR image. According to a study by Lindholm et al., parallel imaging using GRAPPA proved that high-accuracy segmentation and volume measurement are possible in brain MR images [12]. In addition, research to reduce the estimation error by deriving optimized

* Corresponding author. Department of Radiological Science, Gachon University, 191, Hambakmoero, Yeonsu-gu, Incheon, Republic of Korea.
E-mail address: yj20@gachon.ac.kr (Y. Lee).

https://doi.org/10.1016/j.net.2022.09.017
1738-5733/

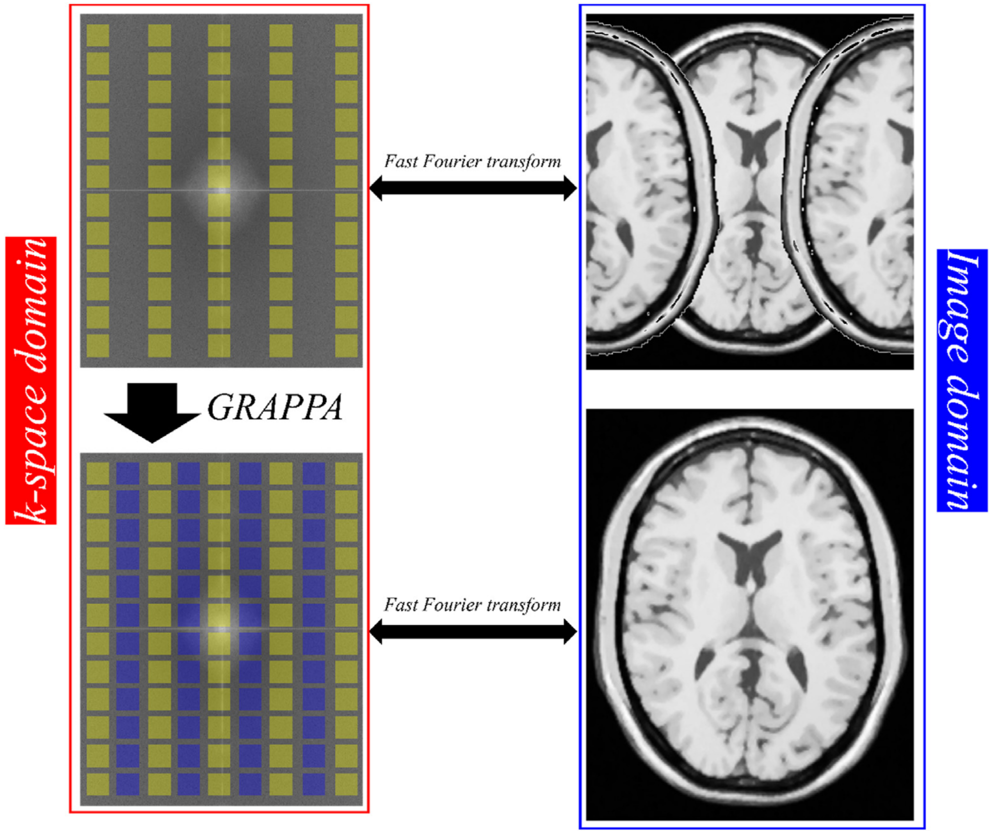

Fig. 1. A simple schematic diagram of the GRAPPA method, a type of parallel imaging. To obtain an MR image with a fast scan time, when the number of samplings in the k-space space is sparsely obtained, aliasing artifacts occur. However, it is the principle of acquiring the final MR image with reduced or no aliasing by supplementing the undersamling parts such as the blue box in the lower left figure. (For interpretation of the references to colour in this figure legend, the reader is referred to the Web version of this article.)

image parameters in GRAPPA diffusion-weighted MRI has been conducted, proving the possibility of various clinical applications [13].

However, when acquiring an MR image using GRAPPA, the signal-to-noise ratio (SNR) is reduced because of the number of coils receiving a signal, and undersampling inevitably occurs [12]. The SNR of the MR image based on parallel imaging, including GRAPPA (SNR_p), is calculated by the following equation, and additional SNR reduction is caused by the acceleration factor (A) and geometry factor (g).

$$SNR_p = \frac{SNR}{g\sqrt{A}} \quad (1)$$

Both A and g in Equation (1) have a large effect on the final SNR loss, and it is difficult to reduce the scan acceleration or reduce the difference between pixels in order to improve the two situations. When the acceleration factor is 2, the SNR decreases about 0.71 times, and the increase in the geometry factor due to the inhomogeneity of the coil decreases the SNR in proportion. The easiest approach to solving these challenges is to utilize denoising software technology. One of the most commonly used software-based filtering methods in medical imaging is the median filter. The median filter is known to be effective when the pixel value of the noise in the image is different from the surrounding pixel value. This filter effectively removes noise using the simple principle of aligning the values for the surrounding pixels and then using the intermediate value as the new value. Based on the median filter, weighted [14], centered [15,16], and adaptive [17] methods have been proposed by several researchers. In particular, Lee proposed a new type of median filtering method based on an improved thresholding method and demonstrated its applicability in functional gamma-ray images using a cadmium zinc telluride detector [18]. However, the aforementioned noise filtering methods have disadvantages in that the efficiency is lowered when the central pixel is noisy or depends on the density value of noise when changing the mask size.

Thus, the application of the improved median filter proposed by Boateng et al. in the principle of selecting an effective median value for each mask using an overlapping mask in the median filter was analyzed to confirm its applicability in PET/MR images using the parallel imaging method with GRAPPA in this study [19]. To analyze the applicability of the proposed improved median filter to the acquired PET/MR images, a conventional median filter was modeled and various image noise levels and no-reference-based evaluation methods were used.

2. Materials and methods

2.1. Used PET/MR fusion imaging system and phantom

In this study, a simultaneous PET/MR fusion imaging system was used (Biography mMR; Siemens Healthineers, Erlangen, Germany). PET/MRI in the form of a circularly arranged detector capable of PET imaging between the radiofrequency (RF) body coil and the gradient coil was used in a magnet composed of a 3.0T main magnetic field.

For image acquisition, a Jaszczak phantom, consisting of six holes of different sizes, was used. Four holes were used for image acquisition, 37 kBq/mL 18F radioisotope was injected into the holes, and the remaining area of the phantom was filled with NaCl + NiSO4 solution (Fig. 2). The imaging parameters for the MR image acquisition using the GRAPPA method are listed in Table 1.

2.2. Modeling of improved median filter

The adaptive median filter uses the principle of changing the filtering mask size according to the noise density, so that only the noise part can be processed. The smaller the mask size of the general filter, the better the image boundary preservation performance; however, the adaptive median filter uses a $(2n+1)\times(2n+1)$ mask, and thus the performance is somewhat lower. In particular, when the mask size of the filter is the maximum value, if the median value is noise, the original pixel value is output as is, and the image quality improvement rate is insufficient.

In this study, an improved median filter proposed by Boateng et al. was modeled based on the principle that an effective median value can be applied to the filtered image using an overlapping mask in the filter to address these shortcomings [19]. The proposed filtering method fixes the mask size and the median value is modeled differently from the middle value of the aligned pixel values. Based on the mask size determination process of the adaptive median filter, the value of n was changed to $\frac{k^2-1}{2}$ ($k = 3, 5, 7, \ldots$).

Fig. 3 shows a schematic diagram of the overall process of improved median filtering using the sample values of the input and output masks. Assuming a mask size of 3×3 with pixel values ranging from 0 to 255, sorting was first performed from the smallest to the largest. In the example in Fig. 3, the median value is 70, which is selected as the effective median value. Subsequently, the value (R), which is the processing starting point, was set by adjusting the appropriate interval of all values. The final output mask is determined as follows:1. Among the re-sorted values, the smallest value is subtracted from the second smallest value, and if it is greater than R, it is reset to the R value. 2. Subtract the second-largest value from the largest value among the re-sorted values and reset it to the R value if it is greater than R.

Table 1
Specific imaging parameters for the MR image with GRAPPA method.

Imaging parameter	Value
TR (repetition time, ms)	3.60
TE (time to echo, ms)	1.23
FOV (field of view, mm)	500
Acquisition time (sec)	19

2.3. Quantitative evaluation of image quality

To quantitatively evaluate the usefulness of the improved median filter in PET/MR fusion images, the noise level and no-reference-based evaluation parameters were used.

The contrast to noise ratio (CNR) and coefficient of variation (COV) evaluation parameters are one of the most commonly used noise level evaluation parameters in the medical imaging field. In this study, CNR and COV were used to evaluate the noise level of the acquired image, and the calculation formulas are as follows:

$$CNR = \frac{\left|S_{Target} - S_{Background}\right|}{\sqrt{\sigma_{Target}{}^2 + \sigma_{Background}{}^2}} \quad (2)$$

$$COV = \frac{\sigma_{Target}}{S_{Target}} \quad (3)$$

where S_{Target} and σ_{Target} are the mean value and standard deviation, respectively, of the region of interest (ROI) in each target, and $S_{Background}$ and $\sigma_{Background}$ are the mean value and standard deviation, respectively, of the ROI in each background. Fig. 4 shows a schematic diagram of setting ROIs in four holes for the COV and CNR calculations. Two evaluation parameters were calculated by setting each target and background ROI in the four-hole regions.

No-reference-based evaluation parameters were used to evaluate the noise level and the overall quality of the acquired PET/MR fusion images. The natural image quality evaluator (NIQE) and blind/referenceless image spatial quality evaluator (BRISQUE) based on the image quality assessment (IQA) algorithm were used

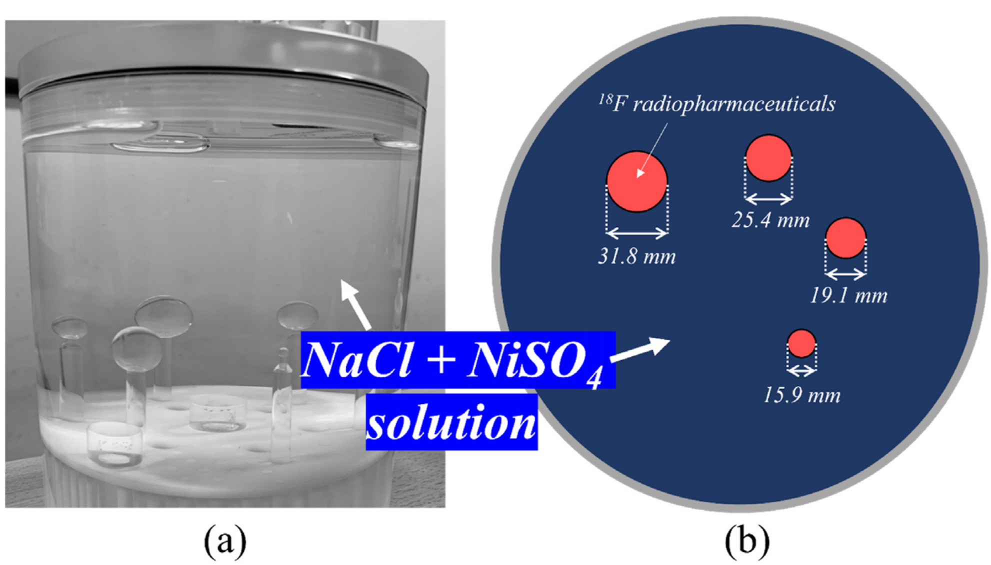

Fig. 2. Photo of (a) the real Jaszczak phantom and (b) a schematic diagram of the phantom viewed from top to bottom. 18F radiopharmaceutical was injected into the four holes of different diameters, and the phantom was filled with NaCl + NiSO4 solution.

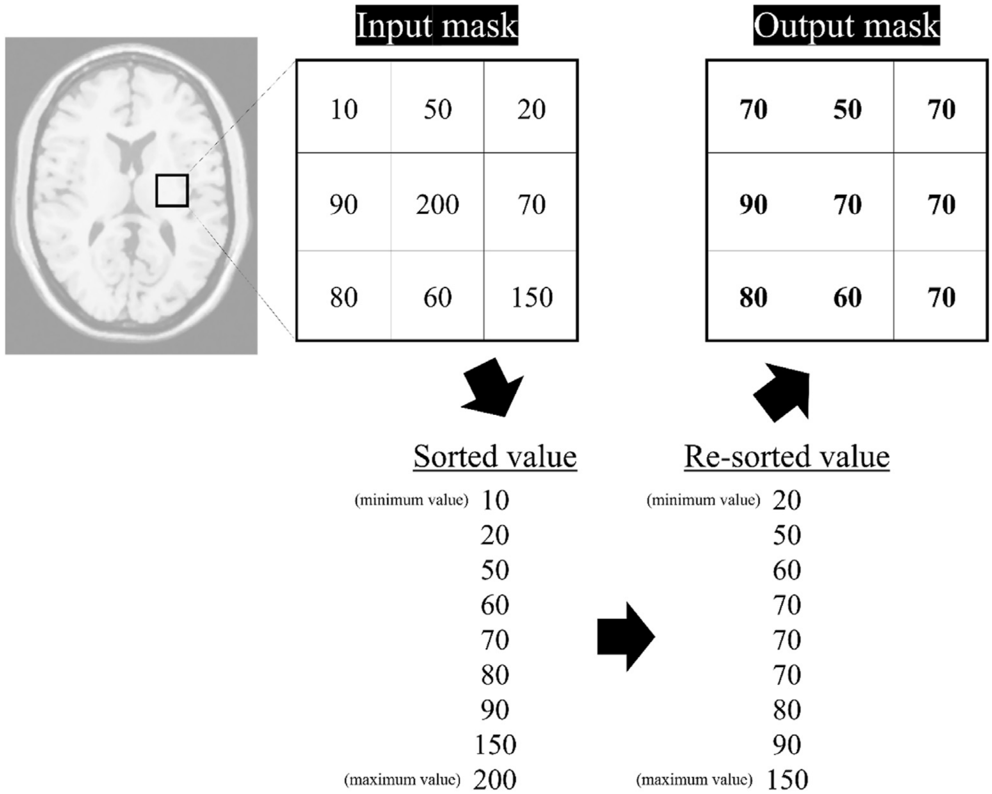

Fig. 3. Simple processing schematic diagram of the proposed improved median filtering (3 × 3 mask size example).

as the no-reference-based evaluation parameters. The NIQE and BRISQUE formulas were completed as follows, based on the principle of matching the generalized Gaussian distribution to the histogram of the MSCN-processed image [20,21].

$$f_{GGD}\left(x; \alpha, \sigma^2\right) = \frac{\alpha}{2\beta\Delta\left(^1/_\alpha\right)} exp\left(-\left(\frac{|x|}{\beta}\right)^\alpha\right) \quad (4)$$

where a is the shape parameter that controls the distribution of σ^2, β is $\sigma\sqrt{\frac{\Delta(^1/_\alpha)}{\Delta(^3/_\alpha)}}$, and Δ is the gamma function.

3. Results and discussion

Fig. 5 shows the PET/MR fusion image obtained based on parallel imaging using GRAPPA and the result of filtering, including an improved median filter. From visual evaluation, we confirmed that the noise in the hot region containing radioactive isotopes was significantly reduced when the proposed improved median filter was applied to the acquired phantom image. In addition, we confirmed that the edge part could be more clearly indicated using the proposed filter compared to the conventional median filter in all hole areas.

Fig. 6 shows the results of the quantitative evaluation of the noise level of the acquired PET/MR fusion images. Fig. 6 (a) shows a graph of the CNR results measured for each acquired image. The CNR results were measured from both the red and yellow circle-shaped ROIs in the target region shown in the sample image in Fig. 4. In all four hole areas, the PET/MR fusion image with the improved median filter showed the best CNR value. The average values of the CNR results measured in the four hole areas were 4.62, 13.27, and 15.37 in the noisy image, conventional median filtered image, and improved median filtered image, respectively. Analysis of the average CNR value showed that 3.32 and 1.16 times improved values were derived in the improved median filtered image compared to the noisy image and the conventional median filtered image, respectively. In particular, we confirmed that as the

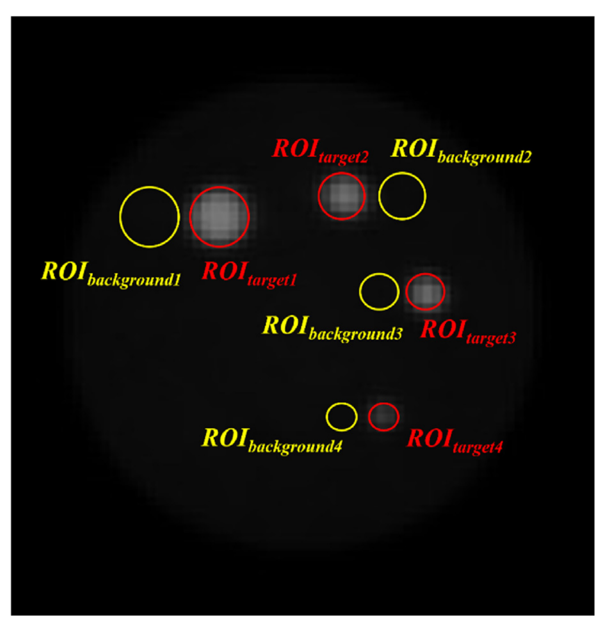

Fig. 4. Schematic diagram of the ROI setting for COV and CNR calculation displayed on the acquired sample PET/MR fusion image.

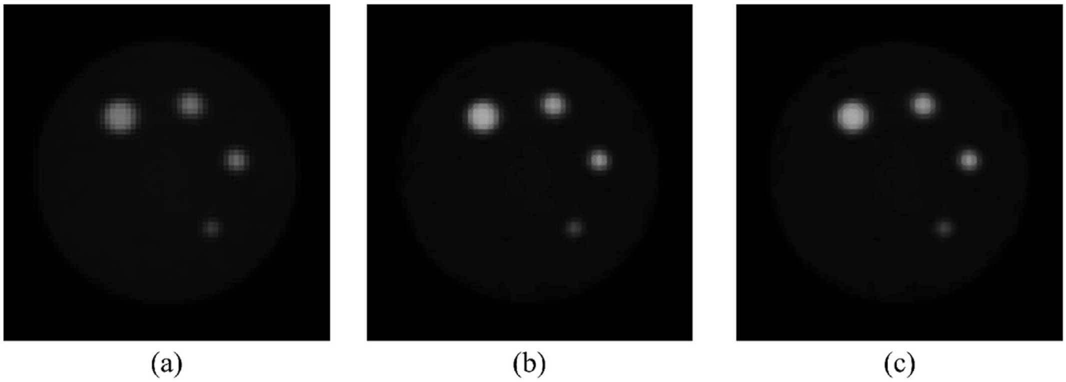

Fig. 5. PET/MR fusion images acquired based on parallel imaging using GRAPPA: (a) noisy image, (b) conventional median filtered image, and (c) improved median filtertered image.

diameter of the hole decreased, the CNR decreased, and the noise improvement rate of the proposed filter also decreased gradually in all three image results. Fig. 6 (b) shows a graph of the COV results measured for each acquired image. The COV results were measured from the red circle-shaped ROIs in the target region shown in the sample image in Fig. 4. In all four hole areas, the PET/MR fusion image with the improved median filter showed the best COV value. The average values of the COV results measured in the four hole areas were 0.380, 0.187, and 0.173 in the noisy, conventional median filtered, and improved median filtered images, respectively. Analysis of the average COV value showed that 2.19 and 1.08 times improved values were derived in the improved median filtered image compared to the noisy image and the conventional median filtered image, respectively. In addition, it was confirmed that in all three result images, as the diameter of the hole decreased, the COV result decreased and the noise improvement rate of the proposed filter also decreased gradually, similar to the trend seen in the CNR results measured previously.

CNR and COV, which are representative parameters for the quantitative evaluation of noise levels, are applied to PET and MR images. In particular, CNR can evaluate contrast and noise simultaneously, and COV can observe signal and noise simultaneously; therefore, both evaluation parameters are widely used in image processing algorithms and filter development research. This research team conducted a study to analyze the applicability of the algorithm using the total variation approach in PET/MR fusion images using CNR and COV [22]. In addition, Part et al. demonstrated the usefulness of a denoising algorithm using a non-local

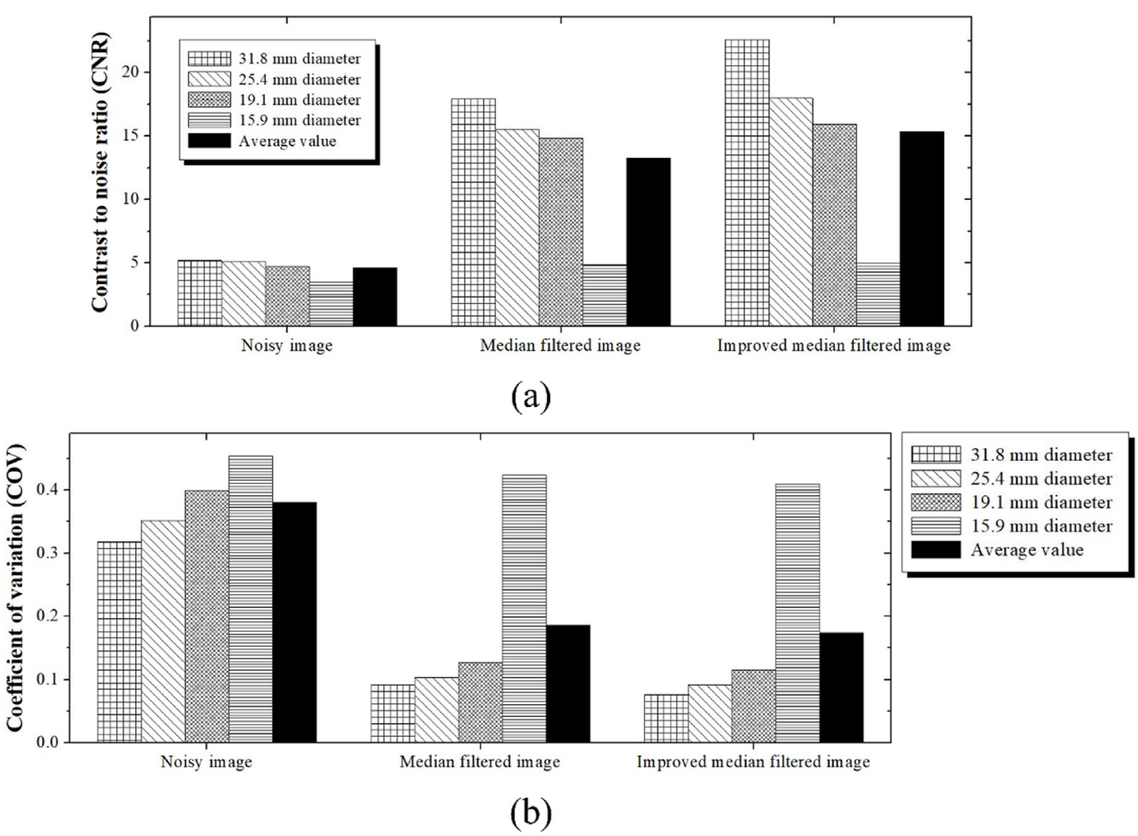

Fig. 6. Result graphs of the (a) CNR and (b) COV results measured for each hole in the acquired PET/MR fusion image.

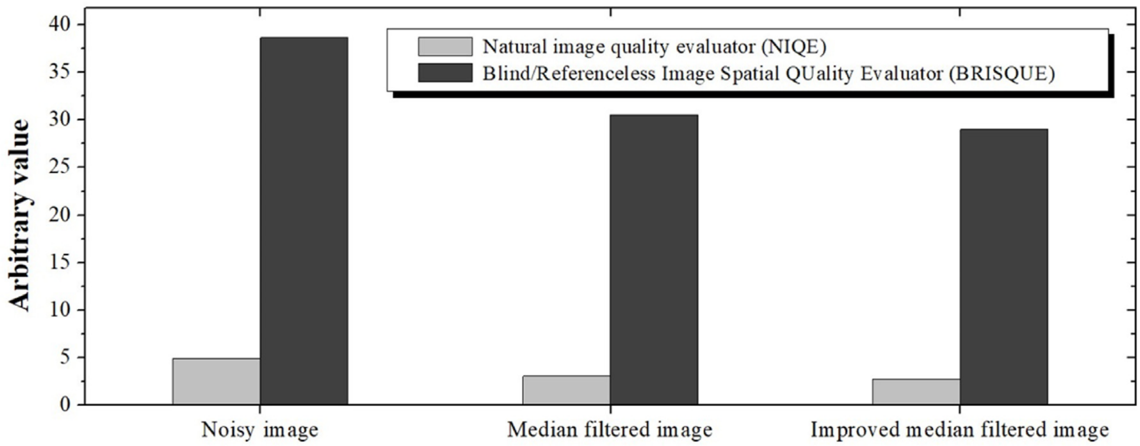

Fig. 7. The no-reference-based evaluation results (NIQE and BRISQUE) measured from acquired PET/MR fusion images.

means approach in diffusion-weighted MR images using high b-values through COV evaluation [23]. In both studies, the accuracy of the evaluation parameters was verified by analyzing the complex image quality changes in the PET or MR images according to the numerical changes in the CNR and COV.

Fig. 7 shows the results of the no-reference-based evaluation, including NIQE and BRISQUE, of the acquired PET/MR fusion images. The evaluated NIQE values are 4.94, 3.06, and 2.75 for the noisy image, conventional median filtered image, and improved median filtered image, respectively. Analysis of the NIQE value showed that 1.79 and 1.11 times improved values were derived in the improved median filtered image than in the noisy image and the conventional median filtered image, respectively. In addition, the evaluated BRISQUE values are 38.66, 30.55, and 29.00 for the noisy image, conventional median filtered image, and improved median filtered image, respectively. Analysis of the BRISQUE value, we demonstrated that 1.33 and 1.05 times improved values were derived in the improved median-filtered image than in the noisy image and the conventional median-filtered image, respectively.

NIQE and BRISQUE are representative non-reference-based evaluation parameters that can evaluate the overall image quality. The smaller the value of both evaluation parameters, the better the image quality. NIQE and BRISQUE are the most used databases for IQA research and are evaluated using the correlation between blurring and noise level of image quality, which is the most prominent in human visual elements. NIQE uses the principle of deriving the characteristics of selected patches for each image and BRISQUE is evaluated by how much the Gaussian image histogram distribution is distorted by blurring or noise [20,21]. When approaching the NIQE and BRISQUE evaluation parameters in the field of medical imaging, researchers can be very useful in the development of denoising algorithms. In particular, when software-based technologies that reduce noise are applied to medical images, blurring inevitably occurs; therefore, parameters that analyze the entire image are required to derive appropriate image quality. Because NIQE and BRISQUE do not use reference images essential for similarity evaluation, they have the advantage of being able to analyze the overall image quality easily. In a study by Kumar, the correlation between the peak signal-to-noise ratio (PSNR) and structural similarity (SSIM), which are representative similarity evaluation factors based on reference images, and BRISQUE were analyzed in brain MR images [24]. In particular, they demonstrated the applicability of no-reference-based evaluation in diagnostic medical imaging by comparing the evaluation tendencies of the SNR and BRISQUE in diffusion-weighted images [23]. In this study, by modeling an improved filtering method, the blurring that inevitably increases with the reduction of noise in the MR image is evaluated in a complex manner.

One of the key aspects of this study is to propose an improved method based on an existing median filter. As mentioned earlier, Boateng et al. proposed the principle of rearranging median values to compensate for the shortcomings of the adaptive median filter. In this study, a new spatial domain approach was presented by applying the modeled improved median filter to the field of diagnostic medical imaging based on the results of the existing digital image analysis. In particular, because signal loss occurs rapidly during PET/MR fusion imaging based on parallel imaging using GRAPPA, it is expected that the proposed improved median filter will be useful, as efficient noise reduction is necessary. GRAPPA is the principle of estimating missing points in k-space and can significantly reduce scan time; however, there is a need to compensate for signal and noise. The GRAPPA type filter has been suggested by many researchers, and the improved median filter proposed in this study is thought to be simple and efficient for various applications. In particular, we expect that a very high lesion detection accuracy can be obtained when the filter modeled in this study is applied to an MR image using high-pass GRAPPA suggested by Huang et al. or non-linear GRAPPA suggested by Chang et al., which can improve noise suppression methods [25–27].

In the future, we believe that the improved median filter can be applied to deep learning technology for MR images. The quality of training or labeling data in the field of MR image reconstruction or the development of ultra-high-resolution algorithms is very important. When constructing these data, a filter or technology that can appropriately enhance blurring and noise can be used to develop a deeper learning method with a higher accuracy. In particular, the improved median filtering method is expected to be much more useful than existing iteration methods in deep learning technology, where time resolution is very important.

4. Conclusion

In this study, the applicability of a PET/MR fusion image based on parallel imaging using GRAPPA was analyzed by modeling a filter with improved noise-removal efficiency based on the conventional median filtering method. In conclusion, the proposed filter is expected to compensate, to some extent, for noise amplification, which is the major problem of parallel imaging including GRAPA.

Declaration of competing interest

The authors declare that they have no known competing financial interests or personal relationships that could have appeared to influence the work reported in this paper.

Acknowledgments

This work was supported by the National Research Foundation of Korea (NRF-2021R1F1A1061440).

References

[1] D. Kim, T. Nam, D. Hernandez, K.N. Kim, Design of rectangular coaxial slot antenna for ultra-highfield magnetic resonance imaging, International Journal of Imaging Systems and Technology 32 (2022) 1133–1142.
[2] Y.D. Son, Y.B. Kim, J.H. Kim, J.H. Kim, D.H. Kwon, H. Lee, Z.H. Cho, Future prospects of positron emission tomography–magnetic resonance imaging hybrid systems and applications in psychiatric disorders, Pharmaceuticals 15 (2022), https://doi.org/10.3390/ph15050583.
[3] S.H. Yoon, S.R. Kim, H.J. Yang, Evaluation of attenuation correction using dixon based bone model for ^{18}F FDG brain PET/MR: a volunteer study, Journal of Magnetics 25 (2020) 463–468.
[4] M.E. Mayerhoefer, H. Prosch, L. Beer, D. Tamandl, T. Beyer, C. Hoeller, D. Berzaczy, M. Raderer, M. Preusser, M. Hochmair, B. Kiesewetter, C. Scheuba, A. Ba-Ssalamah, G. Karanikas, J. Kesselbacher, G. Prager, K. Dieckmann, S. Polterauer, M. Weber, I. Rausch, B. Brauner, H. Eidherr, W. Wadsak, A.R. Haug, PET/MRI versus PET/CT in oncology: a prospective single-center study of 330 examinations focusing on implications for patient management and cost considerations, European Journal of Nuclear Medicine and Molecular Imaging 47 (2020) 51–60.
[5] B. Bybel, R.C. Brunken, F.P. DiFilippo, D.R. Neumann, G. Wu, M.D. Cerqueira, SPECT/CT imaging: clinical utility of an emerging technology, RadioGraphics 28 (2008) 1097–1113.
[6] J.H. Jung, Y. Choi, K.C. Im, PET/MRI: technical challenges and recent advances, Nuclear Medicine and Molecular Imaging 50 (2016) 3–12.
[7] B. Pichler, H.F. Wehrl, A. Kolb, M.S. Judenhofer, PET/MRI: THE NEXT GENERATION OF MULTI-MODALITY IMAGING? Seminars in Nuclear Medicine 38 (2008) 199–208.
[8] M. Blaimer, F.A. Breuer, N. Seiberlich, M.F. Mueller, R.M. Heidemann, V. Jellus, G. Wiggins, L.L. Wald, M.A. Griswold, P.M. Jakob, Accelerated volumetric MRI with a SENSE/GRAPPA combination, Journal of Magnetic Resonance Imaging 24 (2006) 444–450.
[9] J.C. Ye, Compressed sensing MRI: a review from signal processing perspective, BMC Biomedical Engineering 1 (2019), https://doi.org/10.1186/s42490-019-0006-z.
[10] M.A. Griswold, P.M. Jakob, R.M. Heidemann, M. Nittka, V. Jellus, J. Wang, B. Kiefer, A. Haase, Generalized autocalibrating partially parallel acquisitions (GRAPPA), Magnetic Resonance in Medicine 47 (2002) 1202–1210.
[11] S. Aja-Fernandez, G. Vegas-Sanchez-Ferrero, A. Tristan-Vega, Noise estimation in parallel MRI: GRAPPA and SENSE, Magnetic Resonance Imaging 32 (2014) 281–290.
[12] T.L. Lindholm, L. Botes, E.L. Engman, A. Frank, T. Jonsson, L. Svensson, P. Julin, Parallel imaging: is GRAPPA a useful acquisition tool for MR imaging intended for volumetric brain analysis? BMC Medical Imaging 9 (2009) https://doi.org/10.1186/1471-2342-9-15.
[13] Z. Laib, F.A. Sid, K. Abed-Meraim, A. Ouldali, Estimation error bound for GRAPPA diffusion-weighted MRI, Magnetic Resonance Imaging 74 (2020) 181–194.
[14] D.R.K. Brownrigg, The weighted median filter, Communications of the ACM 27 (1984) 807–818.
[15] S.J. Ko, Y.H. Lee, Center weighted median filters and their applications to image enhancement, IEEE Transactions on Circuits and Systems 38 (1991) 984–993.
[16] T. Chen, H.R. Wu, Adaptive impulse detection using center-weighted median filters, IEEE Signal Processing Letters 8 (2001) 1–3.
[17] M. Juneja, R. Mohana, An improved adaptive median filtering method for impulse noise detection, International Journal of Recent Trends in Engineering 1 (2009) 274–278.
[18] Y. Lee, Performance evaluation of noise reduction algorithm with median filter using improved thresholding method in pixelated semiconductor gamma camera system: a numerical simulation study, Nuclear Engineering and Technology 51 (2019) 439–443.
[19] K.O. Boateng, B.W. Asubam, D.S. Laar, Improving the effectiveness of the median filter, International Journal of Electronics and Communication Engineering 5 (2012) 85–97.
[20] A. Mittal, A.K. Moorthy, A.C. Bovik, No-reference image quality assessment in the spatial domain, IEEE Transactions on Image Processing 21 (2012) 4695–4708.
[21] A. Mittal, R. Soundararajan, A.C. Bovik, Making a “completely blind” image quality analyzer, IEEE Signal Processing Letters 20 (2013) 209–212.
[22] C.R. Park, S.H. Kang, Y. Lee, Feasibility of total variation noise reduction algorithm according to various MR-based PET images in a simultaneous PET/MR system: a phantom study, Diagnostics 11 (2021), https://doi.org/10.3390/diagnostics11020319.
[23] J. Park, C.K. Kang, Y. Lee, Quantitative evaluation of the image quality using the fast nonlocal means denoising approach in diffusion-weighted magnetic resonance imaging with high b-value, Journal of the Korean Physical Society 78 (2021) 244–250.
[24] A. Kumar, Nonlocal means image denoising using orthogonal moments, Applied Optics 54 (2015) 8156–8165.
[25] F. Huang, Y.L.S. Vijayakumar, S. Hertel, G.R. Duensing, High-pass GRAPPA: an image support reduction technique for improved partially parallel imaging, Magnetic Resonance in Medicine 59 (2008) 642–649.
[26] Y. Chang, D. Liang, L. Ying, Nonlinear GRAPPA: a kernel approach to parallel MRI reconstruction, Magnetic Resonance in Medicine 68 (2012) 730–740.
[27] S. Madhusoodhanan, J.S. Paul, A quantitative survey of GRAPPA reconstruction in parallel MRI: impact on noise reduction and aliasing, Concepts in Magnetic Resonance A 44A (2015) 287–308.